IEEE Access
Multidisciplinary | Rapid Review | Open Access Journal

Received April 14, 2022, accepted May 9, 2022, date of publication May 16, 2022, date of current version June 2, 2022.

Digital Object Identifier 10.1109/ACCESS.2022.3175322

Optimal Mismatched Filter Design by Combining Convex Optimization With Circular Algorithm

LING JIN, JU WANG, YI ZHONG, AND DUO WANG
School of Information and Electronics, Beijing Institute of Technology, Beijing 100081, China
Corresponding author: Ju Wang (wangju@bit.edu.cn)

This work was supported in part by the National Natural Science Foundation of China under Grant 61971043.

ABSTRACT Mismatched filters (MMF) have been intensively explored for linear-frequency modulation (LFM) waveform sidelobe reduction. Unlike other design strategies, the use of convex optimization (CO) techniques is able to find the optimal design. However, existing studies for CO-based MMF design have focused on minimizing peak sidelobe level (PSL), which might not take the mainlobe widening sacrifice into account. To address this issue, this paper proposes a weighted CO model targeting a flexible tradeoff between sidelobe suppression and mainlobe widening. Moreover, to better control the optimization problem via the presented CO model, the cyclic algorithm (CA) is employed to determine upper limits on mainlobe width. Consequently, the proposed tradeoff MMF design by combining CA with CO would be feasible to meet the requirements of different target detection scenarios. Comprehensive simulations have been carried out to demonstrate the effectiveness of our presented MMF design.

INDEX TERMS Mismatched filter, convex optimization, cyclic algorithm, sidelobe suppression.

I. INTRODUCTION

Linear frequency modulation (LFM) signal is widely used in the modern radar system. Since target detection performance is often adversely affected by the uncertainty of the noise power [1], matched filters (MF) are typically leveraged to improve the signal-to-noise ratio (SNR) without increasing the radar's peak transmitted power [2]. However, high peak sidelobe level (PSL) of MF output tends to cause masking problems between strong and weak targets that come close. Therefore, it is necessary to find a filter design method with better sidelobe suppression performance. If a certain SNR loss is allowed, a filter with better performance of sidelobe suppression can be a candidate [3]. Since this filter has a SNR loss compared with the MF, it is called mismatched filter (MMF). MMF has been extensively investigated in recent studies.

Traditional design methods for MMF can be categorized into two groups: window functions-based and least squares (LS) estimation-based approaches. For the former method, [4]–[6] apply classical weighting window functions to the kernel of the MMF, such as Hamming, Kaiser, or Taylor window functions. Although such methods can suppress range sidelobes to a lower level compared with MF, the sidelobe level is still too high to meet the requirements in some applications [7]. To overcome the problem, the combined window functions have been further proposed [8]–[11]. Nevertheless, they may not be available to control the mainlobe broadening and the SNR loss with only few manually tunable parameters. For the latter method, many studies have intensively investigated to suppress range sidelobes, including least-squares MMF (LS-MMF) [12], iteratively reweighted LS-MMF (IRLS-MMF) [13], diagonally weighted LS-MMF (DWLS-MMF) [14] and iterative weighted LS-MMF (IWLS-MMF) [15]. In spite of the ultra-low sidelobe level, these methods may lead to uncontrollable SNR loss.

Over the past few years, there has been considerable interest in the use of optimization techniques, which has been used in signal processing [16], machine learning [17], [18], wireless communication [19], etc. Since optimization technology can effectively solve the problems mentioned above suffered by traditional design methods, more recent research have exploited optimization techniques to design MMF [20]–[32]. References [20] and [21] apply cyclic algorithm (CA) for MMF design. By terminating the iterative process of CA, the SNR loss and mainlobe broadening of MMF outputs can be effectively controlled. However, CA may not guarantee a globally optimal solution that cannot suppress the sidelobe level to a minimumn [33]. In contrast to CA, CO has the

The associate editor coordinating the review of this manuscript and approving it for publication was Jinming Wen.

advantage of obtaining the best result for the optimization problem. Reference [24] prove that the problem of computing the MMF in regard to the PSL can be formulated as a convex optimization second-order cone programming (SOCP) problem. Based on SOCP, [23], [25] further solve the PSL problem via a convex quadratically constrained quadratic program (QCQP). References [29] and [30] use SOCP and QCQP to jointly design the transmit waveform and MMF, respectively. Reference [31] reduce the power of the interference by using MMF based on SOCP. However, both QCQP and SOCP for MMF design sacrifice the mainlobe widening to minimize PSL, which would likely to deteriorate the range resolution in target detection. Unfortunately, very few articles take mainlobe width into account for CO-based MMF design. Although [32] applies CO with a specific constraint on mainlobe width, this method may not achieve a flexible tradeoff MMF performance between PSL and mainlobe widening. Since the requirement for mainlobe widening varies on the target detection scene, it is unreasonable to impose a fixed value of the mainlobe width.

To tackle the above issue, this paper proposes an MMF design method by combining circular algorithm and convex optimization (CA-CO). Throughout the paper, we aim to construct a CO model targeting a flexible trade-off between PSL and mainlobe widening. First, we construct two CO models that can minimize the PSL and mainlobe width, respectively. Based on the two models, we then construct a multicriterion CO model by means of linear weighting to realize a flexible trade-off MMF performance between PSL and mainlobe widening. Specifically, to better control the optimization problem given in the proposed CO model, a maximum allowable mainlobe width is obtained by CA. Based on numerical simulation, we demonstrate that CA-CO method can control the mainlobe width flexibly and have good performance in the cases of multi-targets. For clarity, we summarize our contributions as follows:

- An Optimal mismatched filter design method by combining CO with CA is proposed. The performance of coherent integration on the CA-CO MMF output is validated by simulations.
- We construct a weighted CO model targeting a flexible tradeoff between sidelobe suppression and mainlobe widening.
- To better control the maximal mainlobe widening sacrifice, CA is employed to determine upper limits on mainlobe width.

The rest of this paper is organized as follows. In section II, we introduce the signal model of MMF. In section III, the proposed CA-CO method are briefly introduced. The simulation results and discussions are given in section IV. The conclusion is presented in section V.

II. SIGNAL MODEL

The LFM signal is a widely used type of large time and band product signal in radar systems [34]. Here, we give a general model of MMF based on the LFM signal. The signal model of the LFM transmitting signal is given as

$$s(t) = \text{rect}\left(t - T_p, T_p\right) \cdot \exp\left[j\pi K\left(t - \frac{T_p}{2}\right)^2\right] \tag{1}$$

$$\text{rect}\left(t, T_p\right) = \begin{cases} 1, |t| \le \frac{T_p}{2} \\ 0, |t| > \frac{T_p}{2} \end{cases} \tag{2}$$

where T_p is the pulse width, $K = B/T_p$ is the rate of frequency change, and B is the bandwidth.

Assuming that the pulse repetition interval (PRI) of the transmitting signal is T and the sampling frequency is f_s, the number of samples for each pulse can be expressed as

$$N = T \cdot f_s. \tag{3}$$

According to (1) and (3), the transmitting signal can be expressed as follows:

$$s(n) = s(t)|_{t=\frac{n}{f_s}}, n = 0, 1, \ldots, N-1. \tag{4}$$

Suppose that there is a point target p at a distance R_p from the radar, its discrete baseband echo $s_r(n)$ with no noise and interference can be represented as

$$\begin{aligned} s_r(n) &= \sigma_p s\left(n - n_p\right) \cdot \exp\left(-j2\pi f_c \tau_p\right) \\ n &= 0, 1, \ldots, N-1 \end{aligned} \tag{5}$$

where σ_p is the backscattering coefficient of the target, f_c is the carrier frequency, $\tau_p = R_p/c$ is the propagation delay between the point target and the radar, and c is the speed of light. $n_p = \tau_p \cdot f_s$ represents the number of samples sampled at f_s for τ_p. Then, the fast Fourier transform (FFT) of (5) is computed, and we obtain

$$\begin{aligned} S_r(k) &= \sigma_p S(k) \cdot \exp\left(-j\frac{2\pi k n_p}{N}\right) \cdot \exp\left(-j2\pi f_c \tau_p\right) \\ k &= 0, 1, \ldots, N-1 \end{aligned} \tag{6}$$

where $S(k)$ denotes the FFT of $s(n)$.

The received echos need to be processed by a filter. The filter coefficients $\mathbf{w}$ are presented as follows:

$$\mathbf{w} = [w(0), w(1), \ldots, w(N-1)]^T \tag{7}$$

where $[\cdot]^T$ denotes the transposition.

The FFT operation on $\mathbf{w}$, the filter coefficients expression $\mathbf{W}$ in the frequency domain, as below:

$$\begin{aligned} \mathbf{W} &= \text{FFT}\{\mathbf{w}\} \\ &= [W(0), W(1), \ldots, W(N-1)]^T. \end{aligned} \tag{8}$$

If $W(k) = S^*(k)$, this filter is MF, where $S^*(k)$ represents the conjugate of $S(k)$. The output of the filter can be written as:

$$\begin{aligned} s_w(n) &= \text{IFFT}\left\{S_r(k)W(k)\right\} \\ &= \sigma_p \text{IFFT}\left\{S(k)W(k) \cdot \exp\left(-j\frac{2\pi k n_p}{N}\right)\right\} \end{aligned} \tag{9}$$

$$\begin{aligned} &\cdot \exp\left(-j2\pi f_c \tau_p\right) \\ &= \sigma_p \mathrm{psf}_{\mathrm{w}}\left(n - n_p\right) \cdot \exp\left(-j2\pi f_c \tau_p\right) \\ \mathrm{psf}_{\mathrm{w}}(n) &= \mathrm{IFFT}\{S(k)W(k)\} \end{aligned} \tag{10}$$

where IFFT{} denotes the inverse FFT. We can infer from (9) and (10) that the PSL and mainlobe width of MMF output depend on $\mathrm{psf}_{\mathrm{w}}(n)$ merely. Therefore, we can design a MMF based on $\mathrm{psf}_{\mathrm{w}}(n)$.

For convenience, (4) can be rewritten in matrix form as

$$\mathbf{s} = [s_0, s_1, \ldots, s_{N-1}]^T . \tag{11}$$

The product of two signals in the frequency domain is equivalent to their circular convolution in the time domain, thus $\mathbf{psf}_{\mathrm{w}}$ is given as

$$\mathbf{psf}_{\mathrm{w}} = \mathbf{\Lambda(s)} \cdot \mathbf{w} \tag{12}$$

$$\Lambda(\mathbf{s}) = \begin{bmatrix} s_{\frac{N}{2}} & s_{\frac{N}{2}+1} & \cdots & s_{N-1} & s_0 & \cdots & s_{\frac{N}{2}-1} \\ s_{\frac{N}{2}+1} & s_{\frac{N}{2}+2} & \ddots & s_0 & s_1 & \ddots & s_{\frac{N}{2}} \\ \vdots & \ddots & \ddots & \vdots & \vdots & \ddots & \vdots \\ s_{N-1} & s_0 & \ddots & s_{\frac{N}{2}-2} & s_{\frac{N}{2}-1} & \ddots & s_{N-2} \\ s_0 & s_1 & \cdots & s_{\frac{N}{2}-1} & s_{\frac{N}{2}} & \cdots & s_{N-1} \\ s_1 & s_2 & \ddots & s_{\frac{N}{2}} & s_{\frac{N}{2}+1} & \ddots & s_0 \\ \vdots & \ddots & \ddots & \vdots & \vdots & \ddots & \vdots \\ s_{\frac{N}{2}-1} & s_{\frac{N}{2}} & \ddots & s_{N-2} & s_{N-1} & \cdots & s_{\frac{N}{2}-2} \end{bmatrix} \tag{13}$$

where $\Lambda(\mathbf{s})$ is the circular convolution matrix of $\mathbf{s}$. When $\mathbf{w} = \mathbf{s}^*$, the output of $\mathrm{psf}_{\mathrm{w}}$ is the MF output, denoted by $\mathbf{psf}_{\mathrm{MF}}$. Therefore, the MF output can be written as:

$$\mathbf{psf}_{\mathrm{MF}} = \Lambda(\mathbf{s}) \cdot \mathbf{s}^* . \tag{14}$$

When the MMF coefficient is defined as $\mathbf{w}_{\mathrm{MMF}}$, the expression of MMF output is given by

$$\mathbf{psf}_{\mathrm{MMF}} = \Lambda(\mathbf{s}) \cdot \mathbf{w}_{\mathrm{MMF}} . \tag{15}$$

Compared to MF, the MMF may result in SNR loss. However, the MMF obtain lower sidelobes at the price of mainlobe widening under the fixed SNR loss condition. In the following, we use the above signal model to design the MMF.

III. CA-CO FOR THE MMF DESIGN

In this section, we first consider the output of CA, which is used as the input and mainlobe width constraint of this CO model. After that, we consider a multicriterion CO model to flexibly control the trade-off between PSL and mainlobe widening.

A. CIRCULAR ALGORITHM

Without considering the SNR loss of the MMF, the ideal MMF output $\mathbf{psf}_{\mathrm{ideal}}$ can be written as [20]:

$$\mathbf{psf}_{\mathrm{ideal}} = \mathbf{m} \odot \mathbf{psf}_{\mathrm{MF}} \tag{16}$$

where $\odot$ is the Hadamard product. $\mathbf{m}$ is a group of weighting coefficients, which are expressed as follows:

$$\begin{aligned} \mathbf{m} &= [m(0), m(1), \ldots, m(k), \ldots, m(N-1)]^T \\ m(k) &= \begin{cases} 1, & k \in \text{ mainlobe} \\ 0, & k \in \text{ others} . \end{cases} \end{aligned} \tag{17}$$

According to (15), the ideal MMF output can be obtained:

$$\mathbf{psf}_{\mathrm{ideal}} = \Lambda(\mathbf{s}) \cdot \mathbf{w}_{\mathrm{MMF}} . \tag{18}$$

Thus, $\mathbf{w}_{\mathrm{MMF}}$ can be solved from the $\mathbf{psf}_{\mathrm{ideal}}$ and $\Lambda(\mathbf{s})$. Considering that $\Lambda(\mathbf{s})$ is not necessarily non-singular, only the least square solution of equation (18) can be found. The least square solution of equation (18) can be written as:

$$\mathbf{w}_{\mathrm{LS}} = \left[\Lambda(\mathbf{s})^H \Lambda(\mathbf{s}) + \sigma \mathbf{I}_N\right]^{-1} \Lambda(\mathbf{s})^H \mathbf{psf}_{\mathrm{ideal}} \tag{19}$$

where $[\cdot]^H$ denotes the Hermitian transpose and $\sigma \mathbf{I}_N$ is a diagonal loading term that is needed to prevent ill-conditioning. Since $\Lambda(\mathbf{s})$ is a Hankel matrix, many fast algorithms can be used to accelerate matrix multiplication and inverse operations, such as divide-and-conquer (DC) algorithm and parallel structured matrix multiplication algorithm (PSMMA) when the dimension of $\Lambda(\mathbf{s})$ is large. Because the least square method may result in a large SNR loss, it is necessary to add a constraint to $\mathbf{w}_{\mathrm{LS}}$. The constraint of $\mathbf{w}_{\mathrm{LS}}$ in CA is that the MMF coefficients $\mathbf{w}_{\mathrm{LS}}$ outside the transmitting signal bandwidth are set to $\mathbf{s}^*$. Thus, we can obtain the expression of the MMF coefficients after adding a constraint:

$$\mathbf{w}_{\mathrm{r}} = \mathbf{F}^{-1}(\mathbf{d}_{\mathrm{in}}^{\mathbf{N}} \mathbf{F} \mathbf{w}_{\mathrm{LS}} + \mathbf{d}_{\mathrm{out}}^{\mathbf{N}} \mathbf{F} \mathbf{s}^*) \tag{20}$$

where $\mathbf{F}$ is the N-point DFT matrix:

$$\mathbf{F} = \begin{bmatrix} 1 & 1 & \cdots & 1 \\ 1 & W_N^1 & \cdots & W_N^{N-1} \\ \vdots & \vdots & \ddots & \vdots \\ 1 & W_N^{N-1} & \cdots & W_N^{(N-1)(N-1)} \end{bmatrix} \tag{21}$$

$$W_N^k = \exp(-j\tfrac{2\pi}{N}k).$$

$\mathbf{F}^{-1}$ is the N-point IDFT matrix. $\mathbf{d}_{\mathrm{in}}^{\mathbf{N}}$ and $\mathbf{d}_{\mathrm{out}}^{\mathbf{N}}$ are two diagonal matrices with dimension $N \times N$, respectively. In the diagonal position of $\mathbf{d}_{\mathrm{in}}^{\mathbf{N}}$, we set 1 for the corresponding positions of the points within the transmitting signal bandwidth and 0 for others. Conversely, we set 1 for the corresponding positions of the points outside the transmitting signal bandwidth and 0 for others on the diagonal of $\mathbf{d}_{\mathrm{out}}^{\mathbf{N}}$.

In terms of $\mathbf{w}_{\mathrm{r}}$, current MMF output is given as

$$\bar{\mathbf{y}}_{\mathrm{MMF}} = \Lambda(\mathbf{s}) \mathbf{w}_{\mathrm{r}} . \tag{22}$$

Then, we get the output of the new ideal MMF based on $\bar{\mathbf{y}}_{\mathrm{MMF}}$, which can be expressed as

$$\bar{\mathbf{y}}_{\mathrm{opt}} = \mathbf{m} \odot \bar{\mathbf{y}}_{\mathrm{MMF}} . \tag{23}$$

After that, we can replace $\mathbf{psf}_{\mathrm{ideal}}$ with $\bar{\mathbf{y}}_{\mathrm{opt}}$ and a new $\mathbf{w}_{\mathrm{LS}}$ can be obtained. Finally the desired coefficients of the

MMF can be achieved by repeat the aforementioned process iteratively. The MMF coefficients $\mathbf{w}_{\mathrm{r}}^{i+1}$ after i-th iteration can be written as below:

$$\mathbf{w}_{\mathrm{r}}^{i+1} = \mathbf{F}^{-1}\left[\mathbf{d}_{\mathrm{in}}^{\mathbf{N}}\mathbf{F}\left(\Lambda(\mathbf{s})^{H}\Lambda(\mathbf{s}) + \sigma\mathbf{I}_{N}\right)^{-1} \Lambda(\mathbf{s})^{H}\mathbf{d}_{\mathrm{m}}^{i}\Lambda(\mathbf{s})\mathbf{w}_{\mathrm{r}}^{i} + \mathbf{d}_{\mathrm{out}}^{\mathbf{N}}\mathbf{F}\mathbf{s}^{*}\right] \tag{24}$$

$$\bar{\mathbf{y}}_{\mathrm{MMF}}^{i} = \Lambda(\mathbf{s})\mathbf{w}_{\mathrm{r}}^{i} \tag{25}$$

where $\mathbf{d}_{\mathrm{m}}^{i}$ is a diagonal matrix defined by $\mathbf{m}$, i denotes the result of the i-th iteration, $\bar{\mathbf{y}}_{\mathrm{MMF}}^{i}$ is CA output of ith iteration. When $i = 1$, $\mathbf{w}_{\mathrm{r}}^{1} = \mathbf{w}_{\mathrm{r}}$.

As the number of iterations increases, CA will cause the mainlobe to widen gradually. Thus, we can flexibly control the mainlobe width of CA result through iterations number. In different target detection scenarios, we can control the mainlobe width of CA output to satisfy different requirements of the upper limit of mainlobe widening by changing iterations number. Because of this feature, it is suitable for CA to be used as the upper limit of mainlobe widening in the CO model. After calculating the number of sampling points within the 3dB mainlobe width (the width of the mainlobe at 3 dB below the mainlobe peak) based on the desired range resolution and sampling rate, we give a stopping criterion as [20]:

$$\mathrm{ML}_{3\mathrm{dB}}(\bar{\mathbf{y}}_{\mathrm{MMF}}^{i}) \leq \varepsilon \tag{26}$$

where $\mathrm{ML}_{3\mathrm{dB}}(\bar{\mathbf{y}}_{\mathrm{MMF}}^{i})$ represents the 3dB mainlobe width of the i-th iterated MMF output, and ε is the number of sampling points within the 3dB mainlobe width. When $\mathrm{ML}_{3\mathrm{dB}}(\bar{\mathbf{y}}_{\mathrm{MMF}}^{i}) > \varepsilon$, the iteration stops. Suppose that the iteration stopping criterion is satisfied when $i = \lambda$, the initial CA-CO MMF coefficients designed by CA is $\mathbf{w}_{\mathrm{CA}} = \mathbf{w}_{\mathrm{r}}^{\lambda}$. Thus, the initial MMF output designed by CA can be given as:

$$\mathbf{y}_{\mathrm{CA}} = \Lambda(\mathbf{s})\mathbf{w}_{\mathrm{CA}} \tag{27}$$

where $\mathbf{y}_{\mathrm{CA}}$ is the output of CA. Thus, the output of CA is suitable to be the mainlobe constraint of the CO model.

B. CONVEX OPTIMIZATION

Since the mainlobe width of the CA output can be affected by the stop criterion, CA can control the sacrifice of the mainlobe to a certain extent. However, CA may not guarantee a globally optimal solution under the iteration stop condition. Hence, in this subsection, we propose a modified CO method to design MMF, which can control the trade-off between PSL and mainlobe widening in the following. CA output is used as the mainlobe width constraint of this CO model. Meanwhile, based on the position of the sidelobe and mainlobe of the CA output $\mathbf{y}_{\mathrm{CA}}$, the optimized mismatched filter output is divided into the sidelobe optimization region and the mainlobe optimization region. Next, we formulate the convex optimization model of the PSL and mainlobe width for the MMF and add some specific constraints to improve the properties of the MMF.

1) PSL CONVEX OPTIMIZATION MODEL

The sidelobe suppression ability of the MMF can be reflected by the PSL. The lower PSL, the stronger the sidelobe suppression ability of the MMF. Therefore, the problem of improving the sidelobe suppression ability of the MMF can be converted to the problem of minimizing the PSL of the MMF. Therefore, an optimization model can be obtained:

$$\begin{aligned} \min_{\mathbf{w}} \quad & \left\|\mathbf{d}_{\mathrm{CA\_SL}}\Lambda(\mathbf{s})\mathbf{w}\right\|_{\infty} \\ \text{s.t.} \quad & \mathbf{s}^{T}\mathbf{w} = \mathbf{s}^{T}\mathbf{s}^{*}. \end{aligned} \tag{28}$$

The optimized vector $\mathbf{w}$ is the MMF coefficients. $\mathbf{d}_{\mathrm{CA\_SL}}$ is a diagonal matrix of ones except for some zero values which correspond to the $\mathbf{y}_{\mathrm{CA}}$ mainlobe position. $\|\mathbf{x}\|_{\infty}$ represents the the infinity norm of vector $\mathbf{x}$. The constraint condition is the peak constraint of the MMF output and prevents the optimization vector $\mathbf{w}$ from being zero.

Because the matched filter maximizes the SNR at the peak response, any other filter will result in a loss in process gain (LPG) at the peak response. Compared with matched filters, LPG will bring SNR loss. LPG is defined as the ratio of the SNR gain of the MMF to the SNR gain of the MF, the expression is as follows [27]:

$$\begin{aligned} \mathrm{LPG} &= 10\log_{10}\left(\frac{\mathrm{SNR}_{\mathrm{MM}}}{\mathrm{SNR}_{\mathrm{M}}}\right) \\ &= 10\log_{10}\left(\frac{\left(\mathbf{s}^{T}\mathbf{w}\right)\left(\mathbf{s}^{T}\mathbf{w}\right)^{H}/\sigma_{n}^{2}\left(\mathbf{w}^{H}\mathbf{w}\right)}{\left(\mathbf{s}^{T}\mathbf{s}^{*}\right)\left(\mathbf{s}^{T}\mathbf{s}^{*}\right)/\sigma_{n}^{2}\left(\mathbf{s}^{T}\mathbf{s}^{*}\right)}\right) \\ &= 10\log_{10}\left(\frac{\left|\mathbf{s}^{T}\mathbf{w}\right|^{2}}{\left(\mathbf{w}^{H}\mathbf{w}\right)\left(\mathbf{s}^{T}\mathbf{s}^{*}\right)}\right) \end{aligned} \tag{29}$$

where $\mathrm{SNR}_{\mathrm{MM}}$ is the SNR gain of the MMF, $\mathrm{SNR}_{\mathrm{M}}$ is the SNR gain of the MF, and σ_n is the variance of the noise. Incorporating the constraints in equation (28) into equation (29), we can get:

$$\mathrm{LPG} = 10\log_{10}\left(\frac{\mathbf{s}^{T}\mathbf{s}^{*}}{\mathbf{w}^{H}\mathbf{w}}\right). \tag{30}$$

According to the definition of LPG, the larger LPG is, the larger the SNR gain of the MMF is. Since the SNR gain of the MF must be greater than that of the MMF, the LPG is always negative. Let $\mathrm{LPG} \geq -10\log_{10}(\eta) = 10\log_{10}\left(\frac{1}{\eta}\right)$, here $\eta > 1$. Then we can get an LPG constraint for MMF:

$$\begin{aligned} \mathrm{LPG} \;&\geq\; 10\log_{10}\left(\frac{1}{\eta}\right) \\ &\Leftrightarrow\; \mathbf{w}^{H}\mathbf{w} \leq \eta\left(\mathbf{s}^{T}\mathbf{s}^{*}\right). \end{aligned} \tag{31}$$

In order to prevent excessive SNR loss of the optimized MMF, we need to limit the LPG of the MMF. The LPG constraints are added into (28). The equivalent optimization model (32) can be obtain:

$$\begin{aligned} \min_{\mathbf{w}} \quad & \left\|\mathbf{d}_{\mathrm{CA\_SL}}\,\Lambda(\mathbf{s})\mathbf{w}\right\|_{\infty} \\ \text{s.t.} \quad & \mathbf{s}^{T}\mathbf{w} = \mathbf{s}^{T}\mathbf{s}^{*} \end{aligned}$$

$$\mathbf{w}^H\mathbf{w} \le \eta\left(\mathbf{s}^T\mathbf{s}^*\right). \tag{32}$$

The CO model (32) minimizes the PSL of MMF output and limited the peak value and the LPG of MMF.

2) MAINLOBE CONVEX OPTIMIZATION MODEL

The MMF causes the mainlobe widening of the output while reducing the sidelobe level of the output. However, the mainlobe width of the MMF output affects the range resolution of the radar. Therefore, it is expected that the mainlobe of the mismatch filter output is as close as possible to the MF output. Therefore, optimization model (33) can be obtained:

$$\begin{aligned}\min_{\mathbf{w}} \quad & \left\|\mathbf{d}_{\mathrm{CA\_ML}}\Lambda(\mathbf{s})\mathbf{w} - \mathbf{d}_{\mathrm{MF}}\mathbf{psf}_{\mathrm{MF}}\right\|_p \\ \text{s.t.} \quad & \mathbf{s}^{\mathrm{T}}\mathbf{w} = \mathbf{s}^T\mathbf{s}^* \\ & \mathbf{w}^H\mathbf{w} \le \eta\left(\mathbf{s}^{\mathrm{T}}\mathbf{s}^*\right).\end{aligned} \tag{33}$$

Here, $\mathbf{d}_{\mathrm{CA\_ML}}$ is the identity matrix minus $\mathbf{d}_{\mathrm{CA\_SL}}$. The diagonal value of $\mathbf{d}_{\mathrm{CA\_ML}}$ is 1 in the position of the $\mathbf{y}_{\mathrm{CA}}$ mainlobe, and 0 in the rest positions. $\mathbf{d}_{\mathrm{MF}}$ is a diagonal matrix with the value of the diagonal elements is 1 or 0. The diagonal value of $\mathbf{d}_{\mathrm{MF}}$ is 1 in the position of the $\mathbf{psf}_{\mathrm{MF}}$ mainlobe, and 0 in the rest positions. $\|\mathbf{x}\|_p$ is the p-norm of the vector $\mathbf{x}$. The p-norm value of the difference between the mainlobe of the MMF and MF output is used to indicate similar degree. Minimize the value of p norm to achieve the effect of optimizing the mainlobe of the MMF output. The PSL and the LPG of MMF are constrained to the desired values.

3) MULTICRITERION CONVEX OPTIMIZATION MODEL

The optimization problem (32) can be optimized to obtain a lower PSL at the price of mainlobe widening. In the same way, the optimization problem (33) can be optimized to obtain a narrow mainlobe width at the price of high PSL. Therefore, it is necessary to formulate a convex optimization model to control the trade-off between PSL and mainlobe widening. We formulate a multicriterion convex optimization model utilizing non-negative linear weighted summation. $f_{\mathrm{SL}}(\mathbf{w})$ and $f_{\mathrm{ML}}(\mathbf{w})$ are used to represent the sidelobe convex optimization function and the mainlobe convex optimization function respectively, where the function expression is:

$$f_{\mathrm{SL}}(\mathbf{w}) = \left\|\mathbf{d}_{\mathrm{CA\_SL}}\Lambda(\mathbf{s})\mathbf{w}\right\|_\infty \tag{34}$$

$$f_{\mathrm{ML}}(\mathbf{w}) = \left\|\mathbf{d}_{\mathrm{CA\_ML}}\Lambda(\mathbf{s})\mathbf{w} - \mathbf{d}_{\mathrm{MF}}\mathbf{psf}_{\mathrm{MF}}\right\|_p. \tag{35}$$

Through linear weighting, we get a new optimization model (36):

$$\begin{aligned}\min_{\mathbf{w}} \quad & \alpha f_{\mathrm{SL}}(\mathbf{w}) + \beta f_{\mathrm{ML}}(\mathbf{w}) \\ \text{s.t.} \quad & \mathbf{s}^{\mathrm{T}}\mathbf{w} = \mathbf{s}^{\mathrm{T}}\mathbf{s}^* \\ & \mathbf{w}^H\mathbf{w} \le \eta(\mathbf{s}^T\mathbf{s}^*)\end{aligned} \tag{36}$$

where α and β are weighting factors that determine the PSL and mainlobe width of MMF output. It is worth noting that the trade-off design is in fact a Pareto optimization [35]. By solving the problem (36), we can bring our solution to the Pareto optimal point. where α and β need to satisfy:

$$\alpha + \beta = 1\alpha \ge 0, \beta \ge 0. \tag{37}$$

When the value of α is too high, it will cause the large sacrifice of the mainlobe widening. To solve this problem, it is necessary to limit the mainlobe width of the optimization result. To facilitate the construction of the mainlobe width constraint, we use the time-delay resolution constant of the mainlobe to reflect the mainlobe width [36]. $A_{\mathrm{opt\_main}}$ and $A_{\mathrm{CA\_main}}$ denote the time-delay resolution constant of CA-CO MMF mainlobe and that of CA result respectively. $A_{\mathrm{opt\_main}}$ and $A_{\mathrm{CA\_main}}$ are written as:

$$A_{\mathrm{opt\_main}} = \frac{\left\|\mathbf{d}_{\mathrm{CA\_ML}}\,\mathbf{\Lambda}(\mathbf{s})\mathbf{w}\right\|_2}{\mathrm{abs}\left(\mathbf{s}^{\mathrm{T}}\mathbf{s}^*\right)} \tag{38}$$

$$A_{\mathrm{CA\_main}} = \frac{\left\|\mathbf{d}_{\mathrm{CA\_ML}}\,\mathbf{\Lambda}(\mathbf{s})\mathbf{w}_{\mathrm{CA}}\right\|_2}{\mathrm{abs}\left(\mathbf{s}^{\mathrm{T}}\mathbf{w}_{\mathrm{CA}}\right)} \tag{39}$$

where abs(·) represents the absolute value, $\mathrm{abs}\left(\mathbf{s}^{\mathrm{T}}\mathbf{s}^*\right)$ represents the peak value of the MMF output after optimization, $\mathrm{abs}\left(\mathbf{s}^{\mathrm{T}}\mathbf{w}_{\mathrm{CA}}\right)$ represents the peak value of the MMF output designed by the CA method.

The mainlobe width can be limited by $A_{\mathrm{opt\_main}} \le A_{\mathrm{CA\_main}}$. Therefore, the optimization model can be obtained (40):

$$\begin{aligned}\min_{\mathbf{w}} \quad & \alpha f_{\mathrm{SL}}(\mathbf{w}) + \beta f_{\mathrm{ML}}(\mathbf{w}) \\ \text{s.t.} \quad & \mathbf{s}^T\mathbf{w} = \mathbf{s}^{\mathrm{T}}\mathbf{s}^* \\ & \mathbf{w}^H\mathbf{w} \le \eta\left(\mathbf{s}^{\mathrm{T}}\mathbf{s}^*\right) \\ & \frac{\left\|\mathbf{d}_{\mathrm{CA\_ML}}\,\mathbf{\Lambda}(\mathbf{s})\mathbf{w}\right\|_2}{\mathrm{abs}\left(\mathbf{s}^{\mathrm{T}}\mathbf{s}^*\right)} \le \frac{\left\|\mathbf{d}_{\mathrm{CA\_ML}}\,\mathbf{\Lambda}(\mathbf{s})\mathbf{w}_{\mathrm{CA}}\right\|_2}{\mathrm{abs}\left(\mathbf{s}^{\mathrm{T}}\mathbf{w}_{\mathrm{CA}}\right)}.\end{aligned} \tag{40}$$

When the value of β is too high, it will cause the large sacrifice of a high sidelobe level. To solve this problem, it is necessary to limit the sidelobe level of the optimization result. So the sidelobe level constraint may be added that the sidelobe level of the MMF output is lower than the sidelobe level of the CA result. Therefore, the optimization model can be obtained (41):

$$\begin{aligned}\min_{\mathbf{w}} \quad & \alpha f_{\mathrm{SL}}(\mathbf{w}) + \beta f_{\mathrm{ML}}(\mathbf{w}) \\ \text{s.t.} \quad & \mathbf{s}^T\mathbf{w} = \mathbf{s}^T\mathbf{s}^* \\ & \mathbf{w}^H\mathbf{w} \le \eta\left(\mathbf{s}^{\mathrm{T}}\mathbf{s}^*\right) \\ & \frac{\left\|\mathbf{d}_{\mathrm{CA\_ML}}\,\mathbf{\Lambda}(\mathbf{s})\mathbf{w}\right\|_2}{\mathrm{abs}\left(\mathbf{s}^{\mathrm{T}}\mathbf{s}^*\right)} \le \frac{\left\|\mathbf{d}_{\mathrm{CA\_ML}}\,\mathbf{\Lambda}(\mathbf{s})\mathbf{w}_{\mathrm{CA}}\right\|_2}{\mathrm{abs}\left(\mathbf{s}^{\mathrm{T}}\mathbf{w}_{\mathrm{CA}}\right)} \\ & \frac{\mathrm{abs}\left(\mathbf{d}_{\mathrm{CA\_SL}}\,\mathbf{\Lambda}(\mathbf{s})\mathbf{w}\right)[i]}{\mathrm{abs}\left(\mathbf{s}^{\mathrm{T}}\mathbf{s}^*\right)} \le \frac{\mathrm{abs}\left(\mathbf{d}_{\mathrm{CA\_SL}}\,\mathbf{\Lambda}(\mathbf{s})\mathbf{w}_{\mathrm{CA}}\right)[i]}{\mathrm{abs}\left(\mathbf{s}^{\mathrm{T}}\mathbf{w}_{\mathrm{CA}}\right)}\end{aligned} \tag{41}$$

where $[i]$ represents the i-th element of the vector.

The CVX toolbox of Matlab was used to solve the optimization problem (41), and MMF coefficient $\mathbf{w}$ was obtained. Thus, the CA-CO can be summarized as follows:

Algorithm 1 CA-CO for MMF Design

Input: Weighting coefficient:α,β
Mainlobe width limitation of CA method:ε
MF output:$\mathbf{psf}_{\mathrm{MF}}$
Ideal MF output:$\mathbf{psf}_{\mathrm{ideal}}$
Allowable LPG:η
Output: MMF coefficient:$\mathbf{w}_{\mathrm{MMF}}$
Processing:
Step1:
get CA result based on ε:
Initialize:$\mathbf{psf}_{\mathrm{new}} \leftarrow \mathbf{psf}_{\mathrm{ideal}}$
$\bar{\mathbf{y}}_{\mathrm{MMF}} \leftarrow \mathbf{psf}_{\mathrm{ideal}}$
While $\mathrm{ML}_{3\mathrm{dB}}(\bar{\mathbf{y}}_{\mathrm{MMF}}) \leq \varepsilon$ **do**
$\mathbf{w}_{\mathrm{LS}} \leftarrow \mathbf{psf}_{\mathrm{new}}$ depended on (19)
Limit $\mathbf{w}_{\mathrm{LS}}$ to get $\mathbf{w}_{\mathrm{r}}$
$\bar{\mathbf{y}}_{\mathrm{MMF}} = \Lambda(\mathbf{s})\mathbf{w}_{\mathrm{r}}$
According to $\bar{\mathbf{y}}_{\mathrm{MMF}}$ to get $\mathbf{m}$
$\mathbf{psf}_{\mathrm{new}} = \mathbf{m} \odot \bar{\mathbf{y}}_{\mathrm{MMF}}$
end
$\mathbf{w}_{\mathrm{CA}} \leftarrow \mathbf{w}_{\mathrm{r}}$
CA result: $\mathbf{y}_{\mathrm{CA}} \leftarrow \Lambda(\mathbf{s})\mathbf{w}_{\mathrm{CA}}$
Step2:
formulate CO model combined with CA :
based on $\mathbf{y}_{\mathrm{CA}}$ sidelobe and mainlobe positions:
$\{\mathbf{d}_{\mathrm{CA\_SL}}, \mathbf{d}_{\mathrm{CA\_ML}}\} \leftarrow \mathbf{y}_{\mathrm{CA}}$
based on $\mathbf{psf}_{\mathrm{MF}}$ mainloe position:
$\mathbf{d}_{\mathrm{MF}} \leftarrow \mathbf{y}_{\mathrm{CA}}$
formulate multicriterion CO function :
$\alpha f_{\mathrm{SL}}(\mathbf{w}) + \beta f_{\mathrm{ML}}(\mathbf{w})$
$f_{\mathrm{SL}}(\mathbf{w}) = \left\|\mathbf{d}_{\mathrm{CA\_SL}}\Lambda(\mathbf{s})\mathbf{w}\right\|_{\infty}$
$f_{\mathrm{ML}}(\mathbf{w}) = \left\|\mathbf{d}_{\mathrm{CA\_ML}}\Lambda(\mathbf{s})\mathbf{w} - \mathbf{d}_{\mathrm{MF}}\mathbf{psf}_{\mathrm{MF}}\right\|_{p}$
add constraints :
- peak level constraint;
- LPG constraint based on η;
- mainlobe constraint based on $\mathbf{y}_{\mathrm{CA}}$;
- sidelobe constraint based on $\mathbf{y}_{\mathrm{CA}}$;

Step3:
use CVX toolbox gets:
MMF coefficient: $\mathbf{w}_{\mathrm{MMF}}$
return $\mathbf{w}_{\mathrm{MMF}}$;

Based on the above description, it is clear that a CO model which has a flexible trade-off between mainlobe widening and PSL is formulated. Meanwhile, we take advantage of the feature that CA can limit the mainlobe width and take the results of CA as the constraint condition of the model to control the maximum allowable mainlobe widening sacrifice.The MMF coefficients can be achieved by solving this the CO model.

TABLE 1. Signal parameters.

Parameters	Values
Pulse width	5μs
Band width	10MHz
PRI	20μs
Sample frequency	102.4MHz

IV. SIMULATION AND ANALYSIS

A. MMF PERFORMANCE INDICATORS

In order to evaluate the performance of the MMF, this paper evaluates the performance of the filter from three aspects: mainlobe widening ratio(MWR), PSLR, and LPG. LPG is defined by (29). Definitions of MWR, PSLR are given below:

MWR of the MMF is defined as the ratio of the null-to-null mainlobe width of MMF output and the null-to-null mainlobe width of MF width [21]. The expression for MWR is as follows:

$$\mathrm{MWR} = \frac{\mathrm{ML}_{\mathrm{MMF}}}{\mathrm{ML}_{\mathrm{MF}}} \tag{42}$$

where $\mathrm{ML}_{\mathrm{MMF}}$ is the null-to-null mainlobe width of the MMF, and $\mathrm{ML}_{\mathrm{MF}}$ is the null-to-null mainlobe width of the MF.

PSLR of the MMF is defined as the ratio of the maximum absolute value of the sidelobe to the peak value of the mainlobe, and the expression is

$$\mathrm{PSLR} = \frac{\max\left|\mathbf{y}_{\mathrm{MMF}} \cdot \mathbf{d}^{\mathbf{N}}\right|}{\max\left|\mathbf{y}_{\mathrm{MMF}}\right|} \tag{43}$$

where $\mathbf{y}_{\mathrm{MMF}}$ denotes the output of the MMF and $\mathbf{d}^{\mathbf{N}}$ is a $N \times N$ diagonal matrix with the position of the mainlobe being 0 and the position of the sidelobe being 1.

B. THE PERFORMANCE OF CA-CO MMF

LFM signal is used for simulation, signal parameters are listed in Table 1.

The linear weighting factors are set as $\alpha = 0.95$ and $\beta = 0.05$, LPG is set as $\eta = -1$. Assume that the maximum allowable range resolution is 18 m, the value of ε is 12. Under the condition of (26), the number of iterations of the CA method is 4. Fig. 1 shows the MF output, CA result, and CA-CO MMF output. It can be inferred from Fig. 1 that CA-CO MMF has a good sidelobe suppression ability. Compared to the CA result which is use as maximum allowable mainlobe widening constraint, it can be easily found that CA-CO MMF output has lower PSL and narrower mainlobe width. To better understand the CA-CO MMF on a fundamental level, Fig. 2 shows the time domain diagram and the frequency domain diagram of the CA-CO MMF.

Based on the discussion in Section III, the number of CA iterations determines the maximum allowable mainlobe widening sacrifice in the CO model. Next, the effect of iterations number on the CA-CO MMF output is analyzed below. The results of the CA iterating 2, 3, and 4 times, respectively,

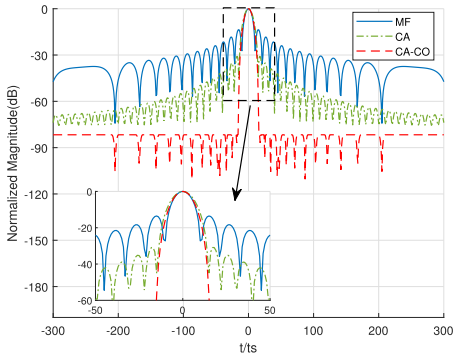

FIGURE 1. MF output,CA result and CA-CO MMF output.

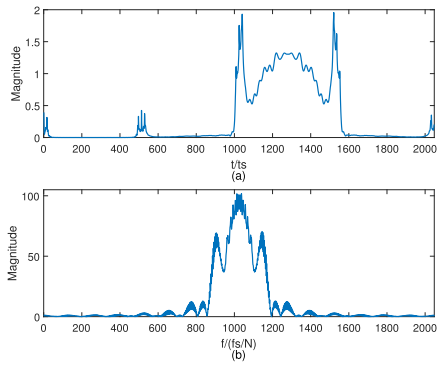

FIGURE 2. (a) The time domain of the CA-CO MMF, (b) the frequency domain of the CA-CO MMF.

are used as the constraints of the CA-CO MMF. The results are shown in Fig. 3. The MWR, PSLR of the CA-CO MMF output are shown in Table 2 under different iterations numbers. We can conclude that the fewer the number of iterations, the smaller the mainlobe width and the larger the PSLR of CA-CO MMF output.

We can flexibly control the trade-off between the PSL and mainlobe widening by selecting the values of α and β. In the case of 4 iterations, α takes 10 values in [0, 1]. Fig. 4 shows the PSLR and the mainlobe width of the CA-CO MMF output with respect to 10 sets of α and β. It can be seen that when the value of α is larger, the ability of sidelobe suppression is stronger, and the mainlobe widening is larger. In contrast, when the value of β is larger, the ability of sidelobe suppression is weaker, and the mainlobe widening is smaller. When α is smaller than 0.7, the PSLR of the CA-CO MMF remains at -32dB because of the sidelobe level constraint based on the CA result in the CO model. The PSLR and MWR of CA-CO MMF output are listed in Table 3 with 5 groups of α and β. The CA-CO MMF output is shown in Fig. 4.

From the above analysis, we conclude that it is able to control the mainlobe widening sacrifice by selecting both CA iteration times and the value of α and β. Under the condition that α and β are constant, the mainlobe width of the CA-CO MMF output decreases with the decreasing iteration times. Under the condition of the fixed maximum mainlobe widening loss, the CA-CO MMF mainlobe widening sacrifice decreases as β increases.

TABLE 2. MWR and PSLR of CA-CO MMF output under different iterations.

Number of CA iterations	MWR of CA-CO	PSLR of CA-CO(dB)
2	1.38	-57.6
3	1.48	-74.4
4	1.57	-81.7

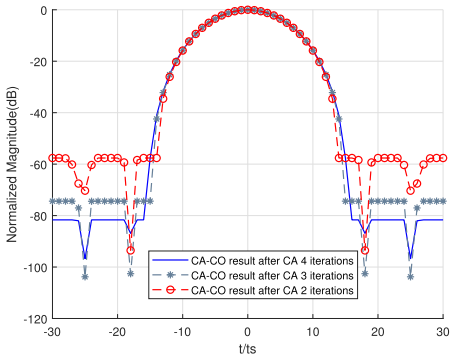

FIGURE 3. MMF output in different iterations under condition $\alpha = 0.95$, $\beta = 0.05$.

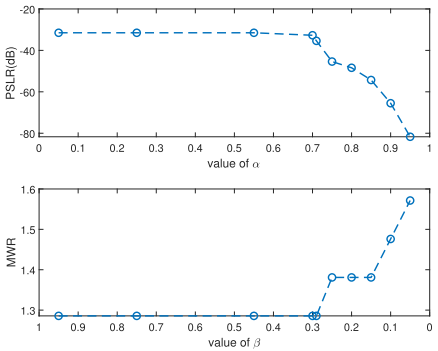

FIGURE 4. PSLR and MWR of CA-CO MMF output for 10 sets of α and β values.

In Fig. 6, the MMF performance comparisons are also performed among CA-CO, CA, and CO. In the legend, it is noted that CA4-CO indicates CA-CO MMF based on 4 CA iterations; CA1-CO indicates CA-CO MMF based on 1 CA iteration; CA10000 indicates CA based on ten thousand iterations; CA1 indicates CA based on 1 iteration. From Table 4, we can see that the LPG of MMF outputs designed by CA4-CO, CA10000, and CO is the same. However, compared with MMF outputs of CA10000 and CO, CA4-CO MMF output has the lowest PSLR, while MWR of it is much smaller than CA MMF output and slightly larger than MWR of CO MMF output. Although the CO MMF output has the smallest MWR, CA-CO can adjust the number of CA iterations and weighting coefficients to achieve the same WMR as CO MMF output, such as CA1-CO MMF output. Similarly, CA can also adjust the iterations number to control the WMR, such as CA1, but its PSLR is much larger than CA1-CO MMF output because of higher LPG. Unfortunately, for CA MMF output, we cannot effectively control LPG to obtain lower PSLR without changing WMR. In general, the CA-CO can flexibly control

TABLE 3. PSLR and MWR of the CA-CO MMF output for different values of α and β.

the value of α and β	MWR	PSLR(dB)
$\alpha = 0.7, \beta = 0.3$	1.29	-32.7
$\alpha = 0.8, \beta = 0.2$	1.38	-48.4
$\alpha = 0.85, \beta = 0.15$	1.48	-54.3
$\alpha = 0.9, \beta = 0.1$	1.48	-65.5
$\alpha = 0.95, \beta = 0.05$	1.57	-81.7

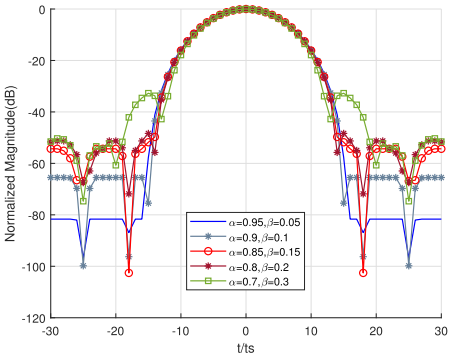

FIGURE 5. CA-CO MMF output designed by different groups of α and β values.

a flexible trade-off between PSL and mainlobe widening and obtain the global optimal solution.

C. TARGET DETECTION BY CA-CO MMF

In this subsection, the coherent integration results of the CA-CO MMF output in the multi-target scenario are discussed below. In this scenario, the number of moving targets is five, and the target parameters are listed in Table 5. The number of integrated pulses is 1024, and the Radon-Fourier transform (RFT) algorithm is used for coherent integration [37].

Figs. 7a-7f show the results of coherent integration in multi-targets scenario of the true scene, MF, CA-CO MMF, CO MMF, CA MMF, and the range dimension result with the velocity of 120 m/s in the absence of noise. From Fig. 7a, there are 5 targets are shown clearly. However, after matched filtering, the small targets are masked by the high range sidelobes of large targets, as shown in Fig. 7b. Fig. 7c shows that CA-CO MMF can suppress the range sidelobes, and five targets can be detected. We can see from Fig. 7d that T_3 cannot be detected from the CO MMF results, because of the high PSLR. Fig. 7e shows the CA MMF result under ten thousand iterations. It can be seen from Fig. 7e that T_2 cannot be detected easily, which demonstrates that the range resolution of the CA MMF result is lower than that of CA-CO MMF result. It can be clearly seen from Fig. 7d that there are five targets in the range dimension of CO-MMF coherent integration result with the velocity of 120 m/s. Unfortunately, five targets cannot all be detected in CA MMF output and CO MMF output due to large mainlobe widening and high PSLR, respectively. The target detection results are listed in Table 6 by measuring the result of coherent integration for CA-CO MMF output. The target detection results show that

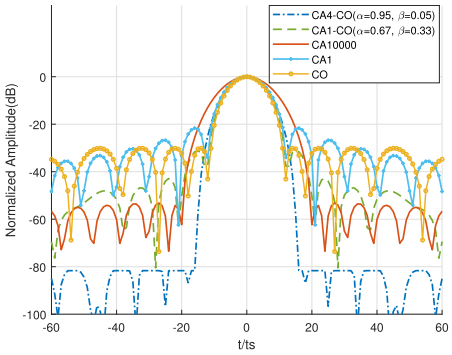

FIGURE 6. MMF output designed by CA4-CO($\alpha = 0.95$, $\beta = 0.05$), CA1-CO($\alpha = 0.67$,$\beta = 0.33$), CA10000, CA1 and CO.

TABLE 4. Performance of MMF output designed by CA-CO, CA and CO.

MMF design method	MWR of MMF	PSLR of MMF(dB)	LPG of MMF(dB)
CA4-CO($\alpha = 0.95, \beta = 0.05$)	1.57	-81.7	-1
CA1-CO($\alpha = 0.67$,$\beta = 0.33$)	1.19	-31.3	-1
CA10000	1.95	-53.2	-1
CA1	1.19	-21.7	-0.3
CO	1.19	-30.1	-1

TABLE 5. Target parameters.

Target index	Target distance(m)	The normalized amplitude (dB)	Target velocity(m/s)
T_0	750	0	120
T_1	766.1	0	120
T_2	720.7	-20	120
T_3	808.6	-30	120
T_4	896.5	-20	120

TABLE 6. Target detection results after coherent integration of CA-CO MMF in the absence of noise.

Target index	Target distance(m)	The normalized amplitude (dB)	Target velocity(m/s)
T_0	748.5	0	120
T_1	767.6	0	120
T_2	720.7	-19.5	120
T_3	808.6	-29.4	120
T_4	896.5	-19.4	120

CA-CO MMF can correctly detect target range and velocity information and result in less peak loss.

Next, we consider the presence of noise in the received signal. Figs. 8a-8d show the results of coherent integration in multi-targets scenario of true scene, CA-CO MMF, MF and the range dimension in velocity is 120 m/s in the presence of noise with SNR $= -2$dB. After calculation, the SNR of the CA-CO MMF output is $10\log_{10}(BT_p) + \eta = 15.98$dB. The gain of coherent integration is 30.1dB. Therefore, the total gain of echo signal after mismatched filtering and coherent integration is 46.08dB. Therefore, the ideal normalized noise base after coherent integration is -44.08dB. After calculation,

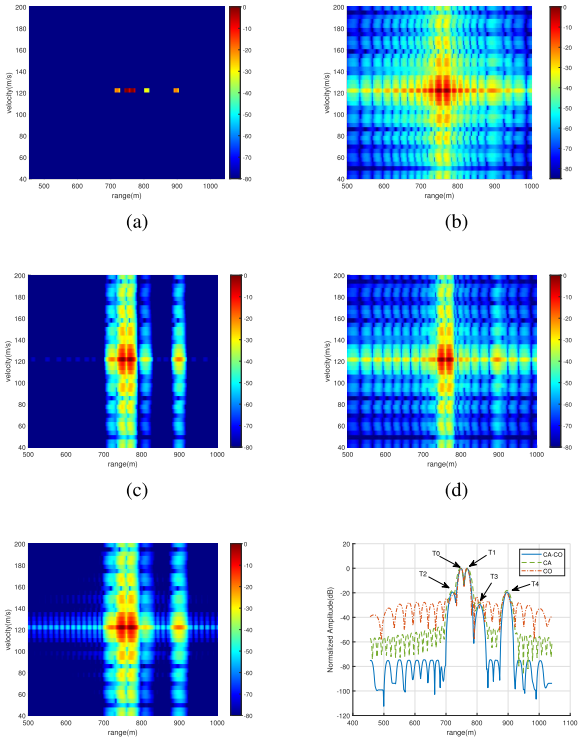

FIGURE 7. Results of RFT coherent integration at 120m/s velocity in multi-targets scenario.(a) true scene; (b) MF; (c) CA-CO MMF; (d) CO MMF; (e) CA MMF; (f) v=120m/s, CA-CO, CO and CA MMF output in the range dimension.

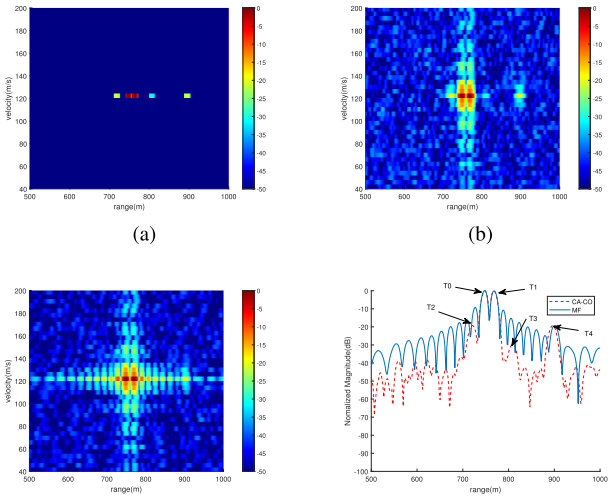

FIGURE 8. Results of RFT coherent integration at 120m/s velocity in multi-targets scenario at SNR=-2dB.(a) true scene;(b) CA-CO MMF; (c) MF; (d) v=120m/s, CA-CO MMF and MF output in the range dimension.

the actual normalized noise base after coherent integration is -43.68dB. It is basically consistent with the theoretical noise base. It can be seen from Fig. 8 that the CA-CO MMF results in less SNR loss and detect the target position well. The target detection results are listed in Table 7 by measuring the result of coherent integration for CA-CO MMF output. The target detection results are basically consistent in the presence and absence of noise.

TABLE 7. Target detection results after coherent integration of CA-CO MMF in the presence of noise.

Target index	Target distance(m)	The normalized amplitude (dB)	Target velocity(m/s)
T_0	748.5	0	120
T_1	767.6	-0.1	120
T_2	720.7	-20.2	120
T_3	808.6	-29.8	120
T_4	896.5	-19.25	120

V. CONCLUSION

In this paper, a CA-CO MMF design method for the LFM signal was proposed. First of all, we proposed that the CA result may be suitable to be the mainlobe widening constraint because it has the feature that the mainlobe of the result can be controlled by iteration numbers. Then, two CO models were formulated to respectively optimize the PSL and mainlobe width. We further designed the MMF via a weighted CO model under both LPG and the maximum allowable mainlobe widening sacrifice constraints, which achieve a flexible trade-off between PSL and mainlobe widening. Numerical results showed that the proposed CA-CO MMF design method can control the mainlobe by weighted coefficients and CA iteration times. Finally, the performance of coherent integration on the CA-CO MMF output was validated by simulations. Simulations showed that accurate information about the velocity and range of the target can be obtained.

Although the proposed CA-CO MMF design method has a good performance for LFM signal with a fixed carrier frequency, it is not suitable for the LFM signal with carrier frequency agility. The MMF design method for LFM signal with carrier frequency agility will be considered in our future work.

REFERENCES

[1] N. Levanon and E. Mozeson, *Radar Signals*. Hoboken, NJ, USA: Wiley, 2004.

[2] J. Ma, K. Li, J. Tian, X. Long, and S. Wu, "Fast sidelobe suppression based on two-dimensional joint iterative adaptive filtering," *IEEE Trans. Aerosp. Electron. Syst.*, vol. 57, no. 5, pp. 3463–3478, Oct. 2021.

[3] Y. Wang, Y. He, S. Sun, and J. Fu, "2D optimal MMF design with a controllable maximum loss for Doppler signals," *IET Radar, Sonar Navigat.*, vol. 12, no. 6, pp. 585–592, Jun. 2018.

[4] S. D. Blunt and E. L. Mokole, "Overview of radar waveform diversity," *IEEE Aerosp. Electron. Syst. Mag.*, vol. 31, no. 11, pp. 2–42, Nov. 2016.

[5] T. Misaridis and J. A. Jensen, "Use of modulated excitation signals in medical ultrasound. Part II: Design and performance for medical imaging applications," *IEEE Trans. Ultrason., Ferroelectr., Freq. Control*, vol. 52, no. 2, pp. 192–207, Feb. 2005.

[6] M. A. Richards, *Fundamentals of Radar Signal Processing*, 2nd ed. New York, NY, USA: McGraw-Hill, 2005.

[7] Z. Ge, P. Huang, and W. Lu, "Matched NLFM pulse compression method with ultra-low sidelobes," in *Proc. Eur. Radar Conf.*, 2008, pp. 92–95.

[8] Z. He and J. Xiang, "A high-performance new combined window weighting method," *J. Signal Process.*, vol. 20, no. 2, pp. 197–200, 2004.

[9] C. Gao and M. Lin, "Sidelobe suppression method of linear frequency modulation pulse pressure signal," *Jiangsu Univ. Sci. Technol., Natural Sci. Ed.*, vol. 30, no. 2, p. 6, 2016.

[10] D. Zhu, X. Dong, and W. Lin, "Pulse compression with very low sidelobes in a spaceborne weather radar," in *Proc. IEEE Int. Geosci. Remote Sens. Symp. (IGARSS)*, vol. 5, Jul. 2008, pp. 252–255.

[11] C. Wang, L. I. Xuehua, Q. Sun, and Z. Qin, "An ultralow side-lobe pulse compression algorithm for frequency-modulated signal," *Mod. Electron. Techn.*, vol. 41, no. 13, p. 5, 2018.
[12] M. Ackroyd and F. Ghani, "Optimum mismatched filters for sidelobe suppression," *IEEE Trans. Aerosp. Electron. Syst.*, vol. AES-9, no. 2, pp. 214–218, Mar. 1973.
[13] J. Kempf and J. A. Jackson, "A modified least-squares mismatched filter for use in radar applications with additive noise," in *Proc. IEEE Int. Radar Conf. (RADAR)*, Apr. 2020, pp. 804–809.
[14] N. Levanon and A. Scharf, "Range sidelobes blanking using contrasting mismatched filters," in *Proc. 16th Int. Conf. Digit. Signal Process.*, Jul. 2009, pp. 1–6.
[15] K. R. Griep, J. A. Ritcey, and J. J. Burlingame, "Poly-phase codes and optimal filters for multiple user ranging," *IEEE Trans. Aerosp. Electron. Syst.*, vol. 31, no. 2, pp. 752–767, Apr. 1995.
[16] J. Wen, Z. Zhou, and H. Chen, "An optimal condition for the block orthogonal matching pursuit algorithm," *IEEE Access*, vol. 6, pp. 38179–38185, 2018.
[17] K. Wu, F. Li, C. Tellambura, and H. Jiang, "Optimal selective transmission policy for energy-harvesting wireless sensors via monotone neural networks," *IEEE Internet Things J.*, vol. 6, no. 6, pp. 9963–9978, Dec. 2019.
[18] Y. Zhong, Y. Yang, X. Zhu, Y. Huang, E. Dutkiewicz, Z. Zhou, and T. Jiang, "Impact of seasonal variations on foliage penetration experiment: A WSN-based device-free sensing approach," *IEEE Trans. Geosci. Remote Sens.*, vol. 56, no. 9, pp. 5035–5045, Sep. 2018.
[19] F. Liu, Y.-F. Liu, A. Li, C. Masouros, and Y. C. Eldar, "Cramér–Rao bound optimization for joint radar-communication beamforming," *IEEE Trans. Signal Process.*, vol. 70, pp. 240–253, 2022.
[20] Y. Sun, Q. Liu, J. Cai, and T. Long, "A novel weighted mismatched filter for reducing range sidelobes," *IEEE Trans. Aerosp. Electron. Syst.*, vol. 55, no. 3, pp. 1450–1460, Jun. 2019.
[21] Y. Sun, H. Fan, E. Mao, Q. Liu, and T. Long, "Range-Doppler sidelobe suppression for pulse-diverse waveforms," *IEEE Trans. Aerosp. Electron. Syst.*, vol. 56, no. 4, pp. 2835–2849, Aug. 2020.
[22] M.-E. Chatzitheodoridi, A. Taylor, O. Rabaste, and H. Oriot, "A sidelobe level minimization mismatched filter using continuous phase frequency-shift keying codes for the off-grid delay problem," in *Proc. 29th Eur. Signal Process. Conf. (EUSIPCO)*, Aug. 2021, pp. 1755–1759.
[23] O. Rabaste and L. Savy, "Mismatched filter optimization via quadratic convex programming for radar applications," in *Proc. Int. Radar Conf.*, Oct. 2014, pp. 1–6.
[24] A. De Maio, Y. Huang, M. Piezzo, S. Zhang, and A. Farina, "Design of radar receive filters optimized according to L_p-norm based criteria," *IEEE Trans. Signal Process.*, vol. 59, no. 8, pp. 4023–4029, Aug. 2011.
[25] O. Rabaste and L. Savy, "Mismatched filter optimization for radar applications using quadratically constrained quadratic programs," *IEEE Trans. Aerosp. Electron. Syst.*, vol. 51, no. 4, pp. 3107–3122, Oct. 2015.
[26] P. J. Kajenski, "Mismatch filter design via convex optimization," *IEEE Trans. Aerosp. Electron. Syst.*, vol. 52, no. 4, pp. 1587–1591, Aug. 2016.
[27] M. M. Pishrow, J. Abouei, and H. Ghaferi, "Design of matched and mismatched filters based on peak sidelobe level minimization," *Radioengineering*, vol. 30, no. 2, pp. 388–395, Jun. 2021.
[28] Y. Wang, Y. He, J. Fu, G. Liang, and N. Zou, "Optimal mismatched filter design with a controllable maximum loss," in *Proc. OCEANS MTS/IEEE Charleston*, Oct. 2018, pp. 1–6.
[29] L. Xu, S. Zhou, and H. Liu, "Simultaneous optimization of radar waveform and mismatched filter with range and delay-Doppler sidelobes suppression," *Digit. Signal Process.*, vol. 83, pp. 346–358, Dec. 2018.
[30] U. Tan, O. Rabastc, C. Adnet, and J.-P. Ovarlez, "A sequence-filter joint optimization," in *Proc. 26th Eur. Signal Process. Conf. (EUSIPCO)*, Sep. 2018, pp. 2335–2339.
[31] T. Aittomäki and V. Koivunen, "Mismatched filter design and interference mitigation for MIMO radars," *IEEE Trans. Signal Process.*, vol. 65, no. 2, pp. 454–466, Jan. 2017.
[32] J. Liu, W. Wang, and H. Song, "Optimization of weighting window functions for SAR imaging via QCQP approach," *Sensors*, vol. 20, no. 2, p. 419, Jan. 2020.
[33] A. N'Guessan and I. C. Geraldo, "A cyclic algorithm for maximum likelihood estimation using Schur complement," *Numer. Linear Algebra Appl.*, vol. 22, no. 6, pp. 1161–1179, Dec. 2015.
[34] L. Kocjancic, A. Balleri, and T. Merlet, "Multibeam radar based on linear frequency modulated waveform diversity," *IET Radar, Sonar Navigat.*, vol. 12, no. 11, pp. 1320–1329, Nov. 2018.
[35] F. Liu, L. Zhou, C. Masouros, A. Li, W. Luo, and A. Petropulu, "Toward dual-functional radar-communication systems: Optimal waveform design," *IEEE Trans. Signal Process.*, vol. 66, no. 16, pp. 4264–4279, Aug. 2018.
[36] Q. Guo, R. Tao, Y. Wang, S. Zhou, and T. Shan, "Algorithm for the nominal resolution in rectangular pulse signal using the ambiguity matrix," *J. Electron., China*, vol. 21, no. 1, pp. 23–32, Jan. 2004.
[37] Z. Sun, X. Li, G. Cui, W. Yi, and L. Kong, "Hypersonic target detection and velocity estimation in coherent radar system based on scaled radon Fourier transform," *IEEE Trans. Veh. Technol.*, vol. 69, no. 6, pp. 6525–6540, Jun. 2020.

LING JIN was born in Jiangsu, China, in 1997. He received the bachelor's degree from the Hebei University of Technology, Tianjin, China, in 2019. He is currently pursuing the M.S. degree in electronics and communication engineering with the Beijing Institute of Technology. His research interest includes radar signal processing.

JU WANG was born in Hebei, China, in 1973. She received the Ph.D. degree in electronic engineering from the Beijing Institute of Technology, Beijing, China, in 2004. She is currently an Associate Professor with the School of Information and Electronics, Beijing Institute of Technology. Her current research interests include signal processing and their applications in radar, satellite navigation, and aerospace TT&C.

YI ZHONG received the Ph.D. degree in information and communication engineering from the Beijing University of Posts and Telecommunications, Beijing, China, in 2017, and the Ph.D. degree in computer science from the University of Technology Sydney, Sydney, NSW, Australia, in 2019. She is currently an Assistant Professor with the School of Information and Electronics, Beijing Institute of Technology, Beijing. Her research interests include signal processing, machine learning, and deep learning.

DUO WANG was born in Hubei, China, in 2000. She received the bachelor's degree from the Minzu University of China, Beijing, China, in 2021. She is currently pursuing the M.S. degree in electronics and communication engineering with the Beijing Institute of Technology. Her research interests include interference detection and signal processing.